Structural Factors Determining Photophysical Properties of Directly Linked Zinc(II) Porphyrin Dimers: Linking Position, Dihedral Angle, and Linkage Length

Sung Cho,[†] Min-Chul Yoon,[†] Jong Min Lim,[†] Pyosang Kim,[†] Naoki Aratani,[‡] Yasuyuki Nakamura,[‡] Toshiaki Ikeda,[‡] Atsuhiro Osuka,*[,‡] and Dongho Kim*[,†]

Spectroscopy Laboratory for Functional π-Electronic Systems and Department of Chemistry, Yonsei University, Seoul 120-749, Korea, and Department of Chemistry, Graduated School of Science, Kyoto University, Kyoto 606-8502, Japan

Received: May 19, 2009; Revised Manuscript Received: June 26, 2009

We have investigated the relationship between the photophysical properties and structures of a series of directly linked zinc(II) porphyrin dimers (***mm*Z2**, ***mb*Z2**, and ***bb*Z2**) using time-resolved spectroscopic measurements and theoretical calculations. Their unique characters such as CT nature and torsional motion are caused by interporphyrin interactions and steric effects, respectively, which can be fully understood in terms of three structural factors: linking position, dihedral angle, and linkage length. The orthogonal geometry and heterolinking of ***mm*Z2** and ***mb*Z2** induce the localized MOs and electron unbalance in the constituent porphyrin units, respectively, and consequently lead to distinct CT characters in spite of their different origin. On the other hand, a small interporphyrin steric hindrance in ***bb*Z2** makes a torsional motion possible around the direct $\beta-\beta'$ linkage in the excited state, which is correlated with the solvent dependence of the fast S_1 fluorescence decay component. On the basis of this work, we can gain further insight into the effect of individual structural factors on the photophysical properties, which provides a firm basis for further understanding of the photophysical properties mainly determined by the structural factors in multiporphyrin systems.

I. Introduction

Considerable efforts have been devoted to the investigation of covalently linked multiporphyrin arrays to materialize efficient molecular photonic and electronic devices such as molecular wires, sensors, gates, transistors, and light harvesting apparatus.[1−9] In this context, there have been numerous attempts to substitute functional groups with different nature, increase the number of porphyrin units, and control interporphyrin interactions by using appropriate covalent linkages to improve functional efficiencies as molecular photonic devices. For example, butadiyne-linked porphyrin arrays with ferrocene and fullerene terminals exhibit an efficient long-range charge transfer as a molecular wire,[10] conjugated porphyrin dimers with high two-photon absorption cross-section values show potential applications in two-photon photodynamic therapy,[11] and windmill- and cyclic-porphyrin arrays exhibit enhanced absorbing abilities and efficient excitation energy transfer processes between the constituent porphyrin units.[12,13]

Since widely used covalent linkages such as phenylene and ethylene do not strongly interact with porphyrin units because of their large energy difference, the intrinsic character of porphyrin can be maintained. However, rigid and short linkages give rise to closely contacted structures to induce strong interporphyrin interactions and consequently the photophysical properties of covalently linked porphyrin arrays are perturbed depending on structural factors such as interporphyrin distance and relative orientation.[14] In this regard, we have been interested in the relationship between photophysical properties and structural factors determined by covalent linkages to gain further insight into the structure/property relationship. Since the molecular structures of covalently linked multiporphyrin arrays can be precisely controlled by an appropriate choice of covalent linkages between constituent units, we are probably able to systematically adjust interporphyrin interactions and subsequent photophysical properties as intended. Along this line, we have systematically investigated a series of directly linked zinc(II) porphyrin dimers (***mm*Z2**, ***mb*Z2**, and ***bb*Z2**) linked through *meso*−*meso*, *meso*−β, and β−β positions, respectively, because they are the simplest porphyrin dimers which have been frequently used as a subunit in the formation of multiporphyrin arrays (Scheme 1).

On the basis of our works, we have revealed that the overall molecular structures of directly linked zinc(II) porphyrin dimers are determined by the linking position and the steric repulsion between the peripheral β-hydrogens adjacent to the direct linkage. As a consequence, their perturbed electronic states and photophysical properties can be fully explained in terms of three structural factors: linking position, dihedral angle, and linkage length. By using various spectroscopic methods and theoretical calculations, we have observed that ***mm*Z2** and ***mb*Z2** exhibit distinct CT states in the excited state caused by the orthogonal geometry and asymmetric linking, respectively, which take a part in the internal conversion process as a deactivation ladder between the S_2 and S_1 states. In contrast, ***bb*Z2** does not exhibit any CT states but shows a structural rearrangement in the excited state presumably due to a small steric hindrance and relatively easy rotation around the direct β−β linkage. Conclusively, the linking position and interporphyrin dihedral angle are critical structural factors to determine the degree of perturbation of photophysical properties and consequently the linking position in multiporphyrin arrays has to be carefully selected because the overall photophysical properties as well as the geometrical molecular structures are largely affected by the interporphyrin

* To whom correspondence should be addressed. E-mail: dongho@yonsei.ac.kr (D.K.); osuka@kuchem.kyoto-u.ac.jp (A.O.).
[†] Yonsei University.
[‡] Kyoto University.

10.1021/jp904666s CCC: $40.75
Published on Web 07/17/2009

SCHEME 1: Schematic Molecular Structures of Directly Linked Zinc(II) Porphyrin dimers

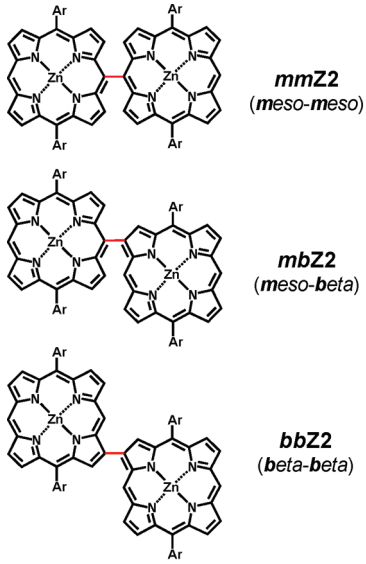

interactions. As a result, an appropriate selection of linking position and linkage nature can be a good strategy to control the overall molecular structures and photophysical properties of multiporphyrin arrays.

II. Experimental Section

Sample Preparation and Steady-State Absorption and Fluorescence Measurements. Porphyrin dimers ***mm*Z2**, ***mb*Z2**, and ***bb*Z2** were prepared according to the reported methods.[15,16] Toluene (spectrophotometric grade, ≥99.5% purity), benzonitrile (anhydrous, 99+% purity), and acetonitrile (spectrophotometric grade, ≥99.5% purity) solvents were purchased from Sigma-Aldrich and used without further purification. UV−vis absorption spectra were recorded with a Cary-5000 UV−vis−NIR spectrometer, and steady-state fluorescence spectra were measured using a Hitachi F-2500 fluorometer.

Nanosecond Time-Resolved Fluorescence Decay Measurements. A time-correlated single-photon counting (TCSPC) system was used for the spontaneous fluorescence decay measurements. The system consisted of a cavity-dumped Kerr lens mode-locked Ti:sapphire laser pumped by a continuous wave Nd:YVO_4 laser (Coherent, Verdi).[13] The second-harmonic beam of the fundamental beam was generated in a 1 mm thick BBO crystal and served as an excitation source. The residual beam was used as a trigger source detected by a fast photodiode. The excitation beam was focused onto a 10 mm thick cuvette containing the sample solution using a 5 cm focal length lens with s polarization. The fluorescence from the sample was collected with a magic angle (54.7°) in order to prevent polarization-dependent signals and focused onto a monochromator (Acton Research) by a 2″ plano-convex lens pair and detected using a microchannel plate photomultiplier tube (Hamamatsu). The full width at half-maximum (fwhm) of the instrument response function obtained for a dilute solution of coffee cream (diffuser) was typically ∼70 ps in our TCSPC system. To obtain the isotropic fluorescence decay profiles, the fluorescence decays were measured at the magic angle (54.7°) using a linear polarizer between the monochromator and the 2″ lens pair. The number of fluorescence photons per unit time was always maintained at <1% of the repetition rate of the excitation pulses, to prevent pile-up distortion in the decay profiles.

Femtosecond Transient Absorption Experiments. The dual-beam femtosecond time-resolved transient absorption (TA) spectrometer consisted of a homemade noncollinear optical parametric amplifier (NOPA) pumped by a Ti:sapphire regenerative amplifier system (Quantronix, Integra-C) operating at 1 kHz repetition rate.[17] The generated visible NOPA pulses had a pulse width of ∼100 fs with an average power of ∼1 mW in the range 500−700 nm which were used as pump pulses. The white-light continuum (WLC) probe pulses were generated using a sapphire window (2 mm thickness) by focusing a small portion of the fundamental pulses which was picked off by a quartz plate before entering the NOPA. The time delay between pump and probe beams was carefully controlled by making the pump beam travel along a variable optical delay (Newport, ILS250). Intensities of the spectrally dispersed WLC probe pulses are monitored by miniature spectrograph (OceanOptics, USB2000+). To obtain the time-resolved transient absorption difference signal (ΔA) at a specific time, the pump pulses were chopped at 25 Hz and absorption spectra intensities were saved alternately with or without pump pulse. Typically, 6000 pulses excite samples to obtain the TA spectra at a particular delay time. The polarization angle between pump and probe beam was set at the magic angle (54.7°) in order to prevent polarization-dependent signals. Cross-correlation fwhm in pump−probe experiments was less than 200 fs, and the chirp of WLC probe pulses was measured to be 800 fs in the 400−800 nm region. To minimize chirp, all reflection optics in the probe beam path and a 2 mm path length of the quartz cell were used.

Femtosecond Time-Resolved Fluorescence Decay Measurements. A femtosecond fluorescence up-conversion system was used for the spontaneous fluorescence decay measurements. The beam source for the B- and Q-state fluorescences were a home-built cavity-dumped Kerr lens mode-locked Ti:sapphire oscillator and a high-power regenerative-amplifier system (Coherent, Clark), respectively.[14a] The second harmonic of the fundamental pulses generated in a 100 μm thick BBO crystal and served as pump pulses. The residual fundamental pulses were used as gate pulses. The pump beam was focused onto a 500 μm thick cuvette containing the sample solution using a 5 cm focal length plano-convex lens with a magic angle (54.7°) in order to prevent polarization-dependent signals. The cuvette was mounted on a motor-driven state and moved constantly back and forth across the beam to minimize photo-degradation. Collecting the fluorescence and focusing it into a BBO crystal for the frequency conversion was achieved by a reflective microscope objective lens (Coherent). We used two kinds of mixing BBO crystals to improve the signal-to-noise ratio. The S_2 fluorescence was measured by using a 0.5 mm crystal to prevent pulse broadening in the mixing crystal. Since the S_1 fluorescence was relatively weak compared with the S_2 fluorescence, we used a 1 mm crystal to improve the signal-to-noise ratio. Therefore, there were two instrument response functions (IRFs) with different time scales. The fwhm of the cross-correlation functions between the scattered pump pulses and the gate pulses were 80 and 300 fs for the S_2 and S_1 fluorescence, respectively.

Theoretical Calculations. We calculated the optimized molecular structures of a series of corroles using DFT with the RB3LYP Hamiltonian and the 6-31G* basis set on a supercomputer (KISTI, IBM p690) and then calculated the singlet excited states using ArgusLab with the *semiempirical* ZINDO Hamiltonian. Although directly linked zinc(II) porphyrin dimers have *t*-butyl groups at the substituted phenyl groups, we calculated dimers without *t*-butyl groups to reduce the job size.

TABLE 1: Optimized Molecular Structures of Directly Linked Zinc(II) Porphyrin Dimers

compound	internal energy/eV	distance/Å	linkage length/Å	dihedral angle[a]/deg	rotational diffusion time[b]/ns	dipole moment/D
***mm*Z2**	−6458.169	8.40	1.51	86.7	0.53	0.000
***mb*Z2**	−6458.176	8.97	1.49	76.2	0.63	0.229
***bb*Z2**	−6458.185	9.88	1.46	44.4	0.69	0.101

[a] Angle between two normal vectors of the mean planes of two constituent porphyrin units. [b] Rotational diffusion time in toluene.

The initial structures of the porphyrin dimers were artificially constructed by two 5,15-diphenyl zinc(II) porphyrins on the basis of the X-ray crystal structure of 5,10,15,20-tetraphenyl zinc(II) porphyrin. We examined several initial structures as dihedral angles between the constituent porphyrin units from 0 to 315° to obtain the optimized structure with the lowest total energy. Additionally, we considered a virtual molecule, 5,15-diphenyl zinc(II) porphyrin (**ZnDPP**), as a theoretical monomer to the quantitative analysis.

III. Results

Optimized Molecular Structures. The optimized molecular structure of ***mm*Z2** is nearly the same as the X-ray structure of *meso*−*meso* linked copper(II) porphyrin dimer which exhibits two nearly planar porphyrin rings with a *meso*−*meso* linkage bond length of 1.51 Å connected in a perpendicular manner and a Cu−Cu distance of 8.34 Å.[18] Although the interporphyrin distance of ***mm*Z2** is slightly longer (Zn−Zn distance 8.40 Å), the overall structure and the *meso*−*meso* linkage length are exactly the same (Table 1, also see the Supporting Information). Accordingly, the employed level of theoretical calculation is adequate and therefore equally suitable to optimize the molecular structures of ***mb*Z2** and ***bb*Z2**. From a structural point of view, as a linking position is shifted from *meso*- to β-carbon, the interporphyrin distance and dihedral angle between the constituent porphyrin units are elongated and reduced, respectively, and concurrently, the bond lengths of the direct linkages in ***mb*Z2** and ***bb*Z2** are shortened. Since the orthogonal geometry of ***mm*Z2** is caused by the steric repulsion between the peripheral β-hydrogens adjacent to the direct *meso*−*meso* linkage, the reduced dihedral angle in ***mb*Z2** and ***bb*Z2** is presumably due to a diminished steric repulsion and an additional energetic benefit by the extended interporphyrin π-conjugation (Table 1). The shorter linkage lengths of ***mb*Z2** and ***bb*Z2** also reflect the reduced dihedral angle and subsequently enhanced electronic communication between the constituent porphyrin units.

Characteristically, ***mb*Z2** and ***bb*Z2** have distinctly large permanent dipole moments in the ground state although **ZnDPP** and ***mm*Z2** are nonpolar (Table 1). Here, it should be noted that the directions of the permanent dipole moments in ***mb*Z2** and ***bb*Z2** are entirely different. While the direction of the permanent dipole of ***bb*Z2** is orthogonal to the long molecular axis and toward the direct $\beta-\beta$ linkage, that of ***mb*Z2** is toward the β-linked porphyrin unit from the *meso*-linked porphyrin unit. Furthermore, the Mulliken charges of the *meso*- and β-linked porphyrin units in ***mb*Z2** were calculated to be +0.040 and −0.040, respectively. Thus, the permanent dipole moment of ***bb*Z2** is caused by an asymmetric geometry but that of ***mb*Z2** is mainly induced by the electron unbalance between the *meso*- and β-linked porphyrin units.

Electron Unbalance of mbZ2. The constituent zinc(II) porphyrin with two *meso*-substituted phenyl groups (**ZnDPP**) exhibits D_{2h} symmetry, and the S_2 and S_1 states are generated by the configurational interactions between four frontier orbitals: two HOMO-like MOs [HOMO-1 (a_u, a_{1u}-like in zinc(II) porphine with D_{4h} symmetry) and HOMO (b_{1u}, a_{2u}-like)] and two LUMO-like MOs [LUMO (b_{3g}, e_{gx}-like) and LUMO+1 (b_{2g}, e_{gy}-like)] (see the Supporting Information).[19] Since the electron density of each frontier MO is highly concentrated on specific sites and clearly divided by nodes between them, the frontier MO interactions in directly linked zinc(II) porphyrin dimers do not simply depend on the interporphyrin distance and relative orientation but also depend on the electron distribution of each coupled MO. In ***mm*Z2** and ***bb*Z2**, two constituent porphyrin units are directly linked at homo *meso*−*meso* and $\beta-\beta$ positions, respectively, and therefore, the homosymmetric MOs with the same energy of the constituent porphyrin units strongly interact with each other (Figure 1). Specifically, the MO interaction between the b_{1u} HOMOs of the constituent porphyrin units in ***mm*Z2** is interrupted because of the orthogonal geometry despite their highly concentrated electron densities at the linked *meso*-carbons. On the contrary, the MO interaction between the a_u HOMO-1s is relatively stronger because of through-space interaction between electron clouds at α- and β-carbons. The coupling energies between the HOMOs and HOMO-1s of the constituent porphyrin units were theoretically evaluated to be 120 and 940 cm^{-1}, respectively, which are well matched with our expectation. As a result, the HOMO and HOMO-3 of ***mm*Z2** are constructed by strong interactions between the HOMO-1s of the constituent porphyrin units and concurrently the HOMO-1 and HOMO-2 are constructed by weak interactions between the HOMOs. In a similar manner, the split MOs of ***mm*Z2** and ***bb*Z2** can be explained by the MO interaction between the homosymmetric MOs of the constituent porphyrin units.

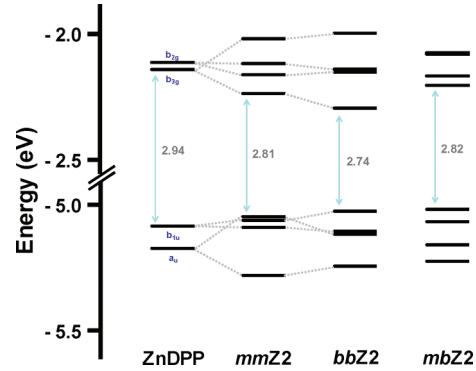

Figure 1. Energetic MO levels of directly linked zinc(II) porphyrin dimers and monomer (**ZnDPP**).

On the other hand, ***mb*Z2** consists of hetero *meso*- and β-linked porphyrin units and the MO interactions are totally different from those of ***mm*Z2** and ***bb*Z2**. In ***mb*Z2**, the MO interactions both between the homosymmetric MOs and between the heterosymmetric MOs of the constituent porphyrin units are inadequate due to a mismatched electron distribution and an energetic difference, respectively. For instance, the b_{1u} HOMO of the constituent *meso*-linked porphyrin unit in ***mb*Z2** does not strongly interact with both the b_{1u} HOMO and a_u HOMO-1 of the constituent β-linked porphyrin unit because the linked

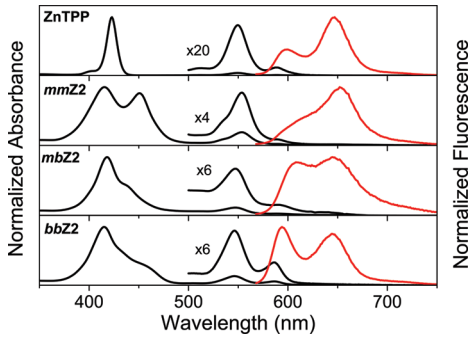

Figure 2. Steady-state absorption and fluorescence spectra in toluene.

β-carbon corresponds to a node and the energy levels of coupled MOs are different, respectively, and subsequently, the electron localized MO at the *meso*-linked porphyrin unit becomes the HOMO of ***mb*Z2**. Similarly, the other frontier MOs of ***mb*Z2** also show localized electron distribution and especially the HOMO-level frontier MOs exhibit the distinct electron localization presumably because of the larger energetic difference between the HOMO and HOMO-1 of the constituent porphyrin unit (see the Supporting Information).

Here, it should be noted that the HOMO of ***mb*Z2** is mainly constructed by the b_{1u} HOMO of the constituent *meso*-linked porphyrin unit. The electrons in the HOMO are the most loosely bound, and the b_{1u} HOMO of the *meso*-linked porphyrin unit exhibits a highly concentrated electron cloud at the linked *meso*-carbon. On the other hand, the b_{1u} HOMO of the β-linked porphyrin unit exhibits a node at the linked β-carbon. Thus, the *meso*-linked porphyrin unit acts as an electron donor in ***mb*Z2** and consequently a part of electron density is probably shifted to the β-linked porphyrin unit. Conclusively, we have proposed that the larger electron density at the β-linked porphyrin unit in ***mb*Z2** and subsequently the strong permanent dipole moment toward the β-linked porphyrin unit are caused by a heterolinking as well as inefficient MO interactions in ***mb*Z2**.

Steady-State Spectroscopic Measurements. Figure 2 shows the steady-state absorption and fluorescence spectra of a series of directly linked zinc(II) porphyrin dimers and tetraphenyl zinc(II) porphyrin (**ZnTPP**) as a reference in toluene. Closely contacted zinc(II) porphyrin dimers exhibit largely split Soret bands because of the large transition dipole moments of the S_2 state in zinc(II) porphyrin monomer and their mutual dipole−dipole interactions. Since the dipole−dipole interaction depends on the relative orientation and the center-to-center distance, we can indirectly obtain information on the 3D structure of porphyrin dimers on the basis of the split Soret bands.[20] As described in the previous studies,[21] ***mm*Z2** with an orthogonal geometry exhibits high- and low-energy Soret bands with a large separation of 1870 cm^{-1} and similar intensity (Table 2). On the other hand, the low-energy Soret bands of ***mb*Z2** and ***bb*Z2** are relatively weak compared with the high-energy Soret bands and especially ***bb*Z2** exhibits at least three Soret bands with the largest band split despite the longest interporphyrin distance among directly linked zinc(II) porphyrin dimers studied here (Table 1). Accordingly, the steady-state absorption spectra of directly linked zinc(II) porphyrin dimers are not simply explained by the exciton coupling model and consequently we have to consider another factor for interporphyrin interactions which will be dealt with in the discussion part.

The S_1 fluorescence spectra of directly linked zinc(II) porphyrin dimers are similar to that of **ZnTPP**. Characteristically, the fluorescence spectra of ***mb*Z2** and ***bb*Z2**, which show the intensified fluorescence around 600 nm (Figure 2), are distinguished from those of ***mm*Z2** and **ZnTPP** and additionally the fluorescence quantum yields of ***mb*Z2** and ***bb*Z2** in toluene are also distinctly large compared with those of ***mm*Z2** and **ZnTPP** (Table 2). Interestingly, while the variation in fluorescence quantum yields of ***mm*Z2** and ***mb*Z2** is similar to that of **ZnTPP**, the fluorescence quantum yield of ***bb*Z2** decreases upon increasing the solvent polarity. Thus, we think that ***mm*Z2** and ***mb*Z2** probably maintain a monomer-like character in the lowest S_1 state but ***bb*Z2** loses it.

Fluorescence Decay Measurements. For the investigation of the exited state dynamics, we measured the S_1 fluorescence decay profiles of directly linked zinc(II) porphyrin dimers in various solvents (see the Supporting Information). Their S_1 fluorescence decay profiles exhibit mostly monoexponential behaviors, and the overall fluorescence lifetimes are gradually reduced upon increasing the solvent polarity. In particular, the S_1 fluorescence lifetime of ***bb*Z2** in acetonitrile is exceedingly reduced by 31 and 36% compared with those in toluene and benzonitrile, respectively.

To quantitatively analyze the energy relaxation dynamics in the S_1 state, we calculated the radiative and nonradiative decay rates using the fluorescence quantum yields and the S_1 fluorescence lifetimes. Consequently, since the nonradiative decay rates of directly linked zinc(II) porphyrin dimers and monomer are nearly 30 times faster than the radiative decay rates presumably due to an efficient intersystem crossing process, the overall S_1 fluorescence lifetimes are mainly determined by the nonradiative decay rates. Nevertheless, the S_1 fluorescence quantum yields of directly linked zinc(II) porphyrin dimers in various solvents are well matched with the radiative decay rates, indicating that the variation of radiative decay rates directly affects the fluorescence quantum yields. Here, the accelerated radiative decay rates of directly linked zinc(II) porphyrin dimers seem to be correlated with the symmetry-lowering effect and subsequently the released prohibition of one-photon transition in the S_1 state. Additionally, the nonradiative decay rates of zinc(II) porphyrin dimers in toluene and benzonitrile are similar to each other but those in acetonitrile are clearly accelerated (Table 2), reflecting different local environment or conformational changes in acetonitrile and subsequently additional deactivation processes.

Transient Absorption Measurements. Figure 3 shows the transient absorption (TA) spectra in various solvents after photoexcitation at 550 nm. Since directly linked zinc(II) porphyrin dimers are directly excited to the S_1 state, we expect that the energy relaxation dynamics from the S_1 state are only shown in TA data. However, the TA spectra of ***mm*Z2** and ***mb*Z2** exhibit a transient excited state absorption (ESA) band around 700 nm and its fast relaxation. While the transient ESA band of ***mm*Z2** is relatively weak and only clearly shown in acetonitrile, that of ***mb*Z2** is shown in all solvents and its amplitude increases upon increasing solvent polarity. As the TA spectra of ***mm*Z2** and ***mb*Z2** after 200 ps are apparently the same and also similar to that of **ZnTPP** (see the Supporting Information), we have suggested that the transient states are rapidly relaxed to the lowest excited state which probably exhibits monomer-like character. On the other hand, ***bb*Z2** does not show any transient ESA bands in the TA spectra and the overall TA spectral features of ***bb*Z2** are also distinguished from those of ***mm*Z2** and ***mb*Z2**. Accordingly, the lowest excited state of ***bb*Z2** is also likely to differ from those of the other dimers.

The ESA decay profiles around 700 nm of ***mm*Z2** in benzonitrile and acetonitrile exhibit fast decay components with time constants of 9.4 and 38.9 ps, respectively, and its amplitude

TABLE 2: Photophysical Properties of Directly Linked Zinc(II) Porphyrin Dimers

compound	solvent	λ_A/nm	λ_F/nm	Stokes shift/cm^{-1}	S_1 state lifetime/ns	Φ_F[a]	$k_r/10^7$ s^{-1}	$k_{nr}/10^8$ s^{-1}
ZnTPP	toluene	423, 549, 588	600, 647	326	2.14	0.033	1.54	4.52
	benzonitrile	429, 559, 600	609, 660	241	2.04	0.040	1.96	4.71
	acetonitrile	421, 555, 596	604, 656	239	2.00	0.030	1.50	4.85
***mm*Z2**	toluene	415, 452, 552, 588	612, 654	686	2.02	0.039	1.54	4.52
	benzonitrile	423, 459, 564, 602	630, 670	736	1.97	0.043	1.96	4.71
	acetonitrile	417, 451, 560, 594	622, 663	736	1.81	0.029	1.50	4.85
***mb*Z2**	toluene	417, 439, 546, 587, 641	605, 646	512	2.13	0.051	1.93	4.76
	benzonitrile	422, 443, 556, 598, 648	620, 660	590	1.99	0.055	2.18	4.86
	acetonitrile	416, 437, 553, 593, 644	616, 655	616	1.76	0.030	1.60	5.36
***bb*Z2**	toluene	414, 433, 453, 545, 586	595, 644	272	2.36	0.077	2.39	4.46
	benzonitrile	419, 437, 458, 555, 592	605, 654	363	2.44	0.053	2.76	4.75
	acetonitrile	412, 431, 454, 552, 589	602, 651	355	1.79	0.036	1.70	5.51

[a] Fluorescence quantum yield (reference: ZnTPP (0.033) in toluene).

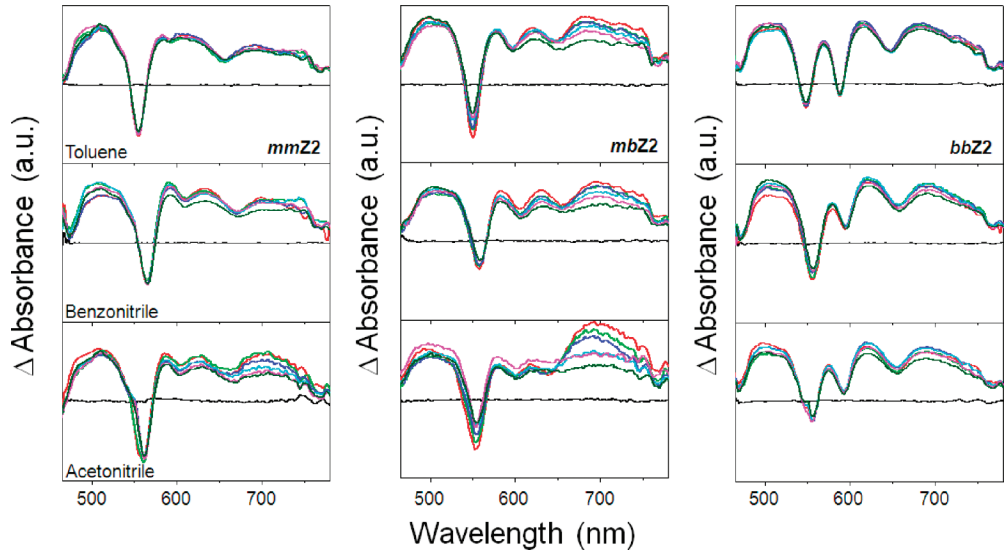

Figure 3. Transient absorption spectra in various solvents after photoexcitation at 550 nm at several time delays from −2 to 200 ps.

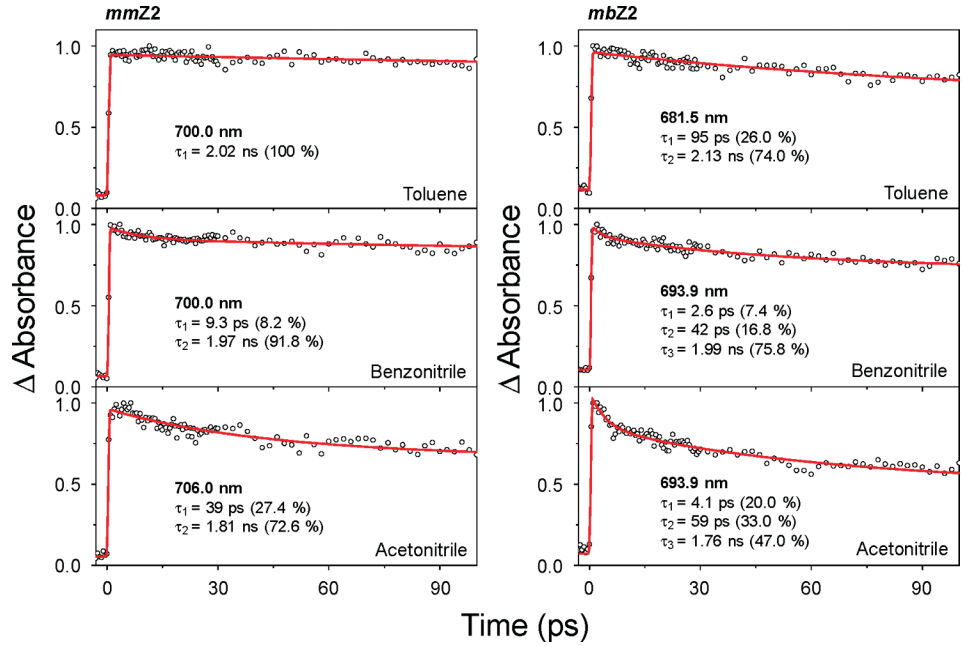

Figure 4. Transient absorption changes around 700 nm of ***mm*Z2** and ***mb*Z2** after photoexcitation at 550 nm.

is enlarged in acetonitrile (Figure 4). Similarly, ***mb*Z2** exhibits fast decay components of several tens of picoseconds in the ESA decay profiles in all solvents and uniquely the third decay component with a few picosecond scale is additionally shown in benzonitrile and acetonitrile. Collectively, the amplitudes of these fast decay components of ***mm*Z2** and ***mb*Z2** increase upon increasing solvent polarity. On the basis of the previous studies on porphyrins,[22] the strong transient ESA band around 700 nm

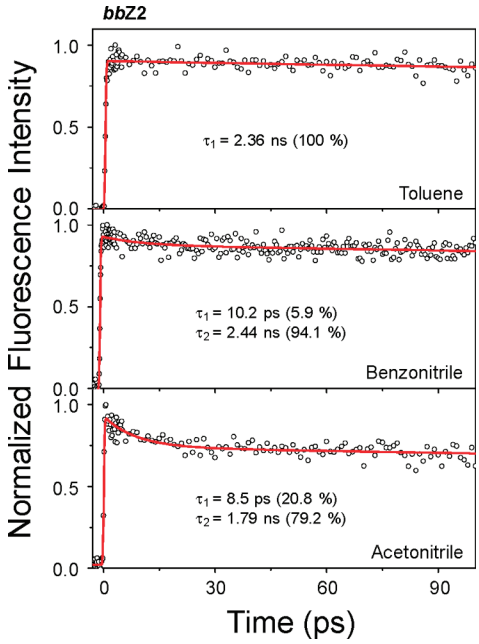

Figure 5. S_1 fluorescence decay profiles around 650 nm of ***bb*Z2** after photoexcitation at 400 nm.

is likely to be characteristic of porphyrin cation species. The origin of the transient states of ***mm*Z2** and ***mb*Z2** will be dealt with in the discussion part.

Fluorescence Up-Conversion Measurements. To obtain further information on the energy relaxation dynamics in the excited states, we measured the S_2 and S_1 fluorescence decay profiles at 450 and 650 nm, respectively, after photoexcitation at 400 nm. At first, the S_2 fluorescence of directly linked zinc(II) porphyrin dimers in toluene rapidly disappears within 100 fs and the corresponding S_1 fluorescence is also impulsively shown, indicative of an efficient internal conversion between the S_2 and S_1 states probably mediated by intermediate electronic states between them.

Interestingly, the S_1 fluorescence decay profiles of ***mm*Z2** and ***mb*Z2** exhibit a rise component of several tens of picoseconds which is well correlated with the fast decay components shown in Figure 4 (see the Supporting Information). As a consequence, the transient states shown in the TA spectra of ***mm*Z2** and ***mb*Z2** can be assigned as one of the intermediate states between the S_2 and S_1 states, taking part in the internal conversion process. However, the major population of the S_1 states of ***mm*Z2** and ***mb*Z2** is impulsively generated and accordingly the internal conversion through the transient state is probably a minor deactivation pathway.

On the other hand, the S_1 fluorescence decay profiles of ***bb*Z2** do not show any fast rise components but exhibit an additional decay component of a few picoseconds, as shown in Figure 5. We have paid attention to the solvent dependence of the decay time constants and amplitudes of the fast S_1 fluorescence decay components, which become slower and larger upon increasing solvent viscosity and polarity, respectively. To reveal the origin of these fast S_1 fluorescence decay components in ***bb*Z2**, we obtained the optimized molecular structure in the lowest excited state on the basis of CIS calculation. Consequently, we found that the interporphyrin dihedral angle of ***bb*Z2** in the lowest excited state is distinctly reduced without any other distinct structural changes, indicating the possibility of a torsional motion in the excited state (see the Supporting Information). Accordingly, we have suggested that the fast S_1 fluorescence decay components in ***bb*Z2** are probably caused by the structural rearrangement mainly due to a torsional motion in the excited state.[23] A small steric hindrance of ***bb*Z2** makes the torsional motion possible around the direct $\beta-\beta'$ linkage in the excited state, and therefore, both the decay time and the amplitude of fast S_1 fluorescence decay components in ***bb*Z2** are directly affected by the solvent. The measured excited state lifetimes of a series of directly linked zinc(II) porphyrin dimers and **ZnTPP** are summarized in Table 3.

IV. Discussion

Directly linked zinc(II) porphyrin dimers can be structurally defined by three factors: linking position, interporphyrin dihedral angle, and linkage length. To quantitatively investigate the effects of individual structural factors on the electronic states and energy relaxation dynamics, we have calculated 20 singlet excited states using ArgusLab with the *semiempirical* ZINDO Hamiltonian, and consequently, the transition energy, oscillator strength, and state dipole moment of each excited state can be obtained. Here, it should be mentioned that we used the state dipole moment, which quantitatively represents the degree of electron density variation between the ground and excited states, as an important criterion of CT character in the excited state. In these calculations, we used the simplified structures of ***mm*Z2**, ***mb*Z2**, and ***bb*Z2** without phenyl substituents to simplify our theoretical analysis, and conclusively, their molecular structures are only determined by three structural factors on the basis of the DFT-based optimized molecular structures. The simulated absorption spectra of simplified ***mm*Z2**, ***mb*Z2**, and ***bb*Z2** are well matched with the steady-state absorption spectra, indicating that the excited states can be explained by two constituent porphyrin units and that the effect of phenyl substituents on the excited state is not significant and consequently that the employed calculations of simplified zinc(II) porphyrin dimers are appropriate for our purpose. For a comparative analysis, we have additionally calculated two kinds of virtual zinc(II) porphyrin dimers with orthogonal geometry and elongated linkage length (see the Supporting Information). The orthogonal zinc(II) porphyrin dimers are used to compare the effects of dihedral angle and linking position simultaneously. On the other hand, since the linkage-elongated zinc(II) porphyrin dimers are linked by a single bond of 1.54 Å, the through-linkage π-orbital interaction is probably not allowed and thus we can compare the effects of interporphyrin distance and through-linkage interactions simultaneously.

The simulated absorption spectra of simplified ***mm*Z2**, ***mb*Z2**, and ***bb*Z2** shown in Figure 6 reflect that the perturbed electronic states are caused by the interporphyrin MO interactions in the frontier MOs of the constituent porphyrin units. The broken degeneracy of the frontier MOs of zinc(II) porphyrin dimers induces complicated configurational interactions between them, and the resulting split Soret bands are shown in the steady-state absorption spectra. It is noteworthy that the splitting of a_u and b_{2g} MOs of the constituent porphyrin units in ***mm*Z2** is significant, which is explained in terms of through-space π-orbital interactions mediated by nonzero overlap between π-orbitals on the α- and β-carbons of the adjacent porphyrin units (see the Supporting Information).[18] Similarly, the b_{1u} and b_{3g} MOs in ***bb*Z2** strongly interact with each other, which can also be regarded as in-phase and out-of-phase through-space MO interactions, respectively.

Effect of Linking Position. The state dipole moment and electron difference map of simplified zinc(II) porphyrin dimers in the excited states indicate that ***mb*Z2** denotes distinct CT

TABLE 3: Fitted Lifetimes of the S_2 and S_1 States

		transient absorption	S_2 fluorescence	S_1 fluorescence	
		at 700 nm	at 450 nm	at 650 nm	
compound	solvent	decay	decay	rise	decay
***mm*Z2**	toluene	2.02 ns (100%)	55 ± 3 fs (100%)		2.02 ns (100%)
	benzonitrile	9.3 ± 1.3 ps (8.2%), 1.97 ns (92.6%)		7.4 ± 0.8 ps (24.5%)	1.97 ns (100%)
	acetonitrile	39 ± 2 ps (27.4), 1.81 ns (72.6%)		52 ± 6 ps (18.8%)	1.81 ns (100%)
***mb*Z2**	toluene	96 ± 5 ps (26.0%), 2.13 ns (74.0%)	72 ± 3 fs (100%)	100 ± 7 ps (24.7%)	2.13 ns (100%)
	benzonitrile	2.6 ± 0.7 ps (7.4%), 42 ± 3 ps (16.8%), 1.99 ns (75.8%)			1.99 ns (100%)
	acetonitrile	4.1 ± 0.4 ps (20.0%), 59 ± 2 ps (33.0%), 1.76 ns (47.0%)		70 ± 7 ps (12.3%)	1.76 ns (100%)
***bb*Z2**	toluene	2.36 ns (100%)	78 ± 4 fs (100%)		2.36 ns (100%)
	benzonitrile	2.44 ns (100%)			10.2 ± 3.7 ps (5.9%), 2.44 ns (94.1%)
	acetonitrile	1.79 ns (100%)			8.5 ± 1.4 ps (20.8%), 1.79 ns (79.2%)

states with a strong state dipole moment between the S_2 and S_1 states (Scheme 2, also see the Supporting Information). Basically, the CT state can occur in the electronic transition correlated with a localized MO. As previously mentioned, while ***mm*Z2** and ***bb*Z2** have fully delocalized MOs, ***mb*Z2** exhibits predominantly localized MOs because of hetero *meso*-β linking. Consequently, we have assigned the transient state of ***mb*Z2** shown in the TA spectra as a CT state located between the S_2 and S_1 states. Furthermore, the increased ESA amplitude of ***mb*Z2** upon increasing solvent polarity can be understood in terms of the stabilized CT state in polar solvent because the transition energy between the CT and ground states is gradually reduced, satisfying a resonance condition by photoexcitation at 550 nm in TA measurements.

Effect of Dihedral Angle. To clarify the nature of the transient state of ***mm*Z2** in benzonitrile and acetonitrile, we have compared the excited states of ***mm*Z2** with those of orthogonal ***mm*Z2** which might coexist because the torsional total energy minimum is broad at the interporphyrin dihedral angle around 90°.[18] Although the dihedral angle difference between ***mm*Z2** and orthogonal ***mm*Z2** is only 3.3°, orthogonal ***mm*Z2** shows distinct CT states (see the Supporting Information). The orthogonal structure prohibits MO interactions, and subsequently, the degenerated and localized MOs are shown in HOMO and LUMO levels of orthogonal ***mm*Z2**. Thus, we have suggested that the transient state of ***mm*Z2** can also be assigned as a CT state and that the CT states of ***mm*Z2** and ***mb*Z2** are energetically located between the S_2 and S_1 states, acting as a deactivation ladder in the internal conversion processes. Conclusively, the linking position and interporphyrin dihedral angle are important factors in the formation of CT states acting as a deactivation pathway in the internal conversion processes. Additionally, it should also be mentioned that the localized monomeric electronic transitions are responsible for the lowest excited states of orthogonal ***mm*Z2** and ***mb*Z2** (Scheme 2, also see the Supporting Information), indicating that their lowest excited states are similar to monomer. Accordingly, the monomer-like behaviors of ***mm*Z2** and ***mb*Z2** are caused by the inefficient MO interactions between the constituent porphyrin units, leading to the localized monomer-like electronic transitions.

SCHEME 2: Electron Difference Maps of the Calculated S_1 and S_9 States of Directly Linked Zinc(II) Porphyrin Dimers (Blue and Red Indicate Increased and Decreased Electron Densities, Respectively)

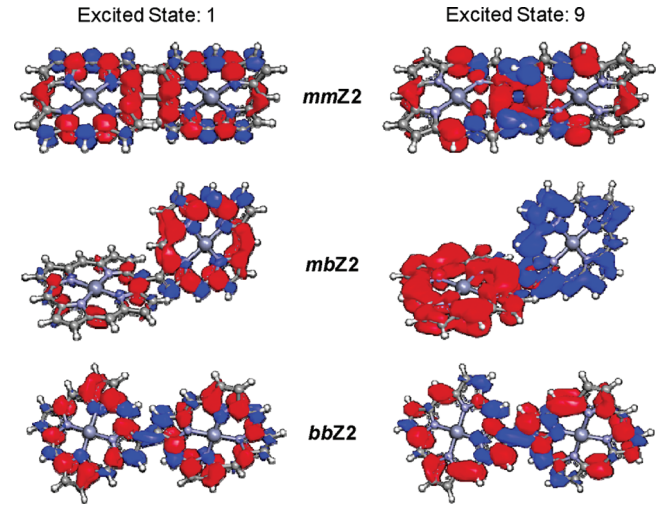

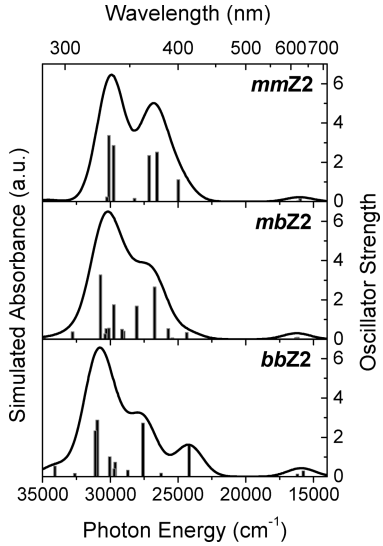

Figure 6. Calculated 20 singlet excited states and simulated absorption spectra of directly linked zinc(II) porphyrin dimers.

We compared the excited states of orthogonal ***bb*Z2** to check whether the orthogonal structure of directly linked zinc(II) porphyrin dimers is an absolute condition for the formation of a CT state or not. Although the simulated absorption spectrum of orthogonal ***bb*Z2** is clearly different from that of ***bb*Z2**, but being similar to those of orthogonal ***mm*Z2** and ***mb*Z2**, orthogonal ***bb*Z2** still does not show any CT states (see the Supporting Information). Although the MO interactions between b_{3g} MOs and between a_u MOs of the constituent porphyrin units in orthogonal ***bb*Z2** are quite weak, all frontier MOs of orthogonal ***bb*Z2** are still fully delocalized because of the through-space MO interactions between highly concentrated electron clouds at the α- and β-carbons adjacent to the linked β-carbons. Accordingly, we have concluded that the MO interactions of the *meso*- and β-linked porphyrins are entirely different because of the unique electron distribution of frontier MOs in the constituent porphyrin unit and therefore the dihedral angle and linking position have to be considered simultaneously.

Effect of Linkage Length. In the linkage-elongated directly linked zinc(II) porphyrin dimers, the simulated absorption spectra show similar absorption spectra to those of the optimized dimers except for a slight perturbation in the low-energy Soret band region (see the Supporting Information). Since ***bb*Z2** has the smallest dihedral angle, the through-linkage interaction in ***bb*Z2** seems to be exceedingly significant among those in directly linked zinc(II) porphyrin dimers, and thus, we representatively compared the MO splittings of optimized and elongated ***bb*Z2**'s. If the through-linkage interaction in ***bb*Z2** is effective, the frontier MOs which exhibit large electron density at the linked β-position interact strongly with each other. The coupling energies of frontier orbitals of the constituent porphyrin units in elongated ***bb*Z2** are averagely reduced by 14% compared with those of ***bb*Z2** and their decrements are nearly the same, indicating that the MO interactions are not affected by the electron distribution of coupled MOs. Consequently, we can suggest that the effect of through-linkage interactions in directly linked zinc(II) porphyrin dimers is insignificant presumably because the dihedral angle of ***bb*Z2** seems to be still too large to induce the interporphyrin interactions mediated by the direct linkage.

V. Conclusions

Although the direct linkage and the through-linkage interaction in directly linked zinc(II) porphyrin dimers seem to play a major role in the interporphyrin interactions, the through-space MO interaction is more important because of their orthogonal structures. On the basis of experimental and theoretical results, we have revealed that the unique behaviors of directly linked zinc(II) porphyrin dimers can be explained in terms of three structural factors. Especially the linking position and dihedral angle strongly affect the interporphyrin interactions and consequently the overall photophysical properties. Additionally, since the electron distributions of frontier MOs of the constituent porphyrin unit are unique and distinctly different from each other, we have to analyze the MO interactions carefully to explain the induced photophysical properties. Importantly, although ***mm*Z2** and ***mb*Z2** exhibit similar transient behaviors in TA data, their origins are totally different. The orthogonal structure and heterolinking of ***mm*Z2** and ***mb*Z2** induce the localized MOs and electron unbalance between the constituent porphyrin units, respectively, leading to the distinct CT character in the excited state. On the other hand, ***bb*Z2** exhibits the structural rearrangement in the excited state because of a small steric repulsion and subsequently an easy rotation around the direct $\beta-\beta$ linkage. Collectively, the structural factors which can be controlled by a rigid covalent linkage strongly affect the interporphyrin interactions and photophysical properties. In this regard, the selection of appropriate linkage and linking position can be a good strategy to fabricate functionalized porphyrin systems for practical applications.

Acknowledgment. This research was financially supported by the Star Faculty and World Class University (2008−1955) Programs of the Ministry of Education, Science, and Technology of Korea and an AFSOR/AOARD grant (FA4869-08-1-4097). The theoretical calculations were performed using the supercomputing resource of the Korea Institute of Science and Technology Information and the ArgusLab 4.0.1 Mark A. Thompson, Planaria Software LLC, Seattle, WA (http://www.arguslab.com). The work at Kyoto University was supported by Grants-in-Aid for Scientific Research (No. 19205006 (A) and No. 20108001 "pi-Space"). S.C., M.-C.Y., J.M.L., and P.K. acknowledge fellowships from the BK21 program of MEST.

Supporting Information Available: Optimized 3D structures of directly linked zinc(II) porphyrin dimers, four frontier MOs of the constituent porphyrin (**ZnDPP**), MO shapes and energies of ***bb*Z2**, S_1 fluorescence decay profiles in various solvents by using TCSPC, transient absorption spectra of **ZnTPP** in toluene, S_1 fluorescence decay profiles around 650 nm of ***mm*Z2** and ***mb*Z2**, simulated absorption spectra upon increasing the dihedral angle, simulated absorption spectra upon increasing the linkage length, electron difference maps of 20 excited states of ***mm*Z2**, electron difference maps of 20 excited states of orthogonal ***mm*Z2**, electron difference maps of 20 excited states of ***mb*Z2**, electron difference maps of 20 excited states of ***bb*Z2**, electron difference maps of 20 excited states of orthogonal ***bb*Z2**, through-space MO interactions in ***mm*Z2**, and the molecular structures of ***bb*Z2** in the ground and lowest excited states using the HF Hamiltonian. This material is available free of charge via the Internet at http://pubs.acs.org.

References and Notes

(1) (a) Bartl, M. H.; Boettcher, S. W.; Frindell, K. L.; Stucky, G. D. *Acc. Chem. Res.* **2005**, *38*, 263. (b) Gust, D.; Moore, T. A.; Moore, A. L. *Acc. Chem. Res.* **2001**, *34*, 40. (c) Szacilowski, K.; Macyk, W.; Drzewiecka-Matuszek, A.; Brindell, M.; Stochel, G. *Chem. Rev.* **2005**, *105*, 2647. (d) de Silva, A. P.; Gunaratne, H. Q. N.; Gunnlaugsson, T.; Huxley, A. J. M.; McCoy, C. P.; Rademacher, J. T.; Rice, T. E. *Chem. Rev.* **1997**, *97*, 1515.

(2) (a) Odobel, F.; Fortage, J. C. R. *Chimie* **2009**, *12*, 437. (b) Holten, D.; Bocian, D. F.; Lindsey, J. S. *Acc. Chem. Res.* **2002**, *35*, 57. (c) Wasielewski, M. R. *Chem. Rev.* **1992**, *92*, 435.

(3) (a) Yeow, E. K. L.; Ghiggino, K. P.; Reek, J. N.; Crossley, M. J.; Bosman, A. W.; Schenning, A. P. H. J.; Meijer, E. W. *J. Phys. Chem. B* **2000**, *104*, 2596. (b) Larsen, J.; Andersson, J.; Polivka, T.; Sly, J.; Crossley, M. J.; Sundström, V.; Åkesson, E. *Chem. Phys. Lett.* **2005**, *403*, 205.

(4) (a) Fujitsuka, M.; Hara, M.; Tojo, S.; Okada, A.; Troiani, V.; Solladie, N.; Majima, T. *J. Phys. Chem. B* **2005**, *109*, 33. (b) Cho, D. W.; Fujitsuka, M.; Sugimoto, A.; Yoon, U. C.; Mariano, P. S.; Majima, T. *J. Phys. Chem. B* **2006**, *110*, 11062. (c) Hara, M.; Samori, S.; Cai, X.; Tojo, S.; Arai, T.; Momotake, A.; Hayakawa, J.; Uda, M.; Kawai, K.; Endo, M.; Fujitsuka, M.; Majima, T. *J. Am. Chem. Soc.* **2004**, *126*, 14217.

(5) (a) Kim, D.; Osuka, A. *J. Phys. Chem. A* **2003**, *107*, 8791. (b) Kim, D.; Osuka, A. *Acc. Chem. Res.* **2004**, *37*, 735. (c) Cho, H. S.; Jeong, D. H.; Cho, S.; Kim, D.; Matsuzaki, Y.; Tanaka, K.; Tsuda, A.; Osuka, A. *J. Am. Chem. Soc.* **2002**, *124*, 14642. (d) Aratani, N.; Cho, H. S.; Ahn, T. K.; Cho, S.; Kim, D.; Sumi, H.; Osuka, A. *J. Am. Chem. Soc.* **2003**, *125*, 9668.

(6) Cho, S.; Li, W.-S.; Yoon, M.-C.; Ahn, T. K.; Jiang, D.-L.; Kim, J.; Aida, T.; Kim, D. *Chem.—Eur. J.* **2006**, *12*, 7676.

(7) (a) Takahashi, R.; Kobuke, Y. *J. Org. Chem.* **2005**, *70*, 2745. (b) Peng, X.; Aratani, N.; Takagi, A.; Matsumoto, T.; Kawai, T.; Hwang, I.-W.; Ahn, T. K.; Kim, D.; Osuka, A. *J. Am. Chem. Soc.* **2004**, *126*, 4468.

(8) (a) Hwang, I.-W.; Kamada, T.; Ahn, T. K.; Ko, D. M.; Nakamura, T.; Tsuda, A.; Osuka, A.; Kim, D. *J. Am. Chem. Soc.* **2004**, *126*, 16187. (b) Hwang, I.-W.; Park, M.; Ahn, T. K.; Yoon, Z. S.; Ko, D. M.; Kim, D.; Ito, F.; Ishibashi, Y.; Khan, S. R.; Nagasawa, Y.; Miyasaka, H.; Ikeda, C.; Takahashi, R.; Ogawa, K.; Satake, A.; Kobuke, Y. *Chem.—Eur. J.* **2005**, *11*, 3753.

(9) (a) Hasobe, T.; Kamat, P. V.; Absalom, M. A.; Kashiwagi, Y.; Sly, J.; Crossley, M. J.; Hosomizu, K.; Imahori, H.; Fukuzumi, S. *J. Phys. Chem. B* **2004**, *108*, 12865. (b) Ayabe, M.; Ikeda, A.; Kubo, Y.; Takeuchi, M.; Shinkai, S. *Angew. Chem., Int. Ed.* **2002**, *41*, 2790.

(10) (a) Winters, M. U.; Dahlstedt, E.; Blades, H. E.; Wilson, C. J.; Frampton, M. J.; Anderson, H. L.; Albinsson, B. *J. Am. Chem. Soc.* **2007**, *129*, 4291. (b) Yoon, D. H.; Lee, S. B.; Yoo, K. H.; Kim, J.; Lim, J. K.; Aratani, N.; Tsuda, A.; Osuka, A.; Kim, D. *J. Am. Chem. Soc.* **2003**, *125*, 11062.

(11) (a) Dahlstedt, E.; Collins, H. A.; Balaz, M.; Kuimova, M. K.; Khurana, M.; Wilson, B. C.; Phillips, D.; Anderson, H. L. *Org. Biomol. Chem.* **2009**, *7*, 897. (b) Kim, K. S.; Lim, J. M.; Osuka, A.; Kim, D. *J. Photochem. Photobiol., C* **2008**, *9*, 13.

(12) (a) Nakano, A.; Osuka, A.; Yamazaki, I.; Yamazaki, T.; Nishimura, Y. *Angew. Chem., Int. Ed.* **1998**, *37*, 3023. (b) Nakano, A.; Osuka, A.; Yamazaki, T.; Nishimura, Y.; Akimoto, S.; Yamazaki, I.; Itaya, A.; Murakami, M.; Miyasaka, H. *Chem.—Eur. J.* **2001**, *7*, 3134.

(13) (a) Cho, H. S.; Rhee, H.; Song, J. K.; Min, C.-K.; Takase, M.; Aratani, N.; Cho, S.; Osuka, A.; Joo, T.; Kim, D. *J. Am. Chem. Soc.* **2003**, *125*, 5849. (b) Hori, T.; Aratani, N.; Takagi, A.; Matsumoto, T.; Kawai, T.; Yoon, M.-C.; Yoon, Z. S.; Cho, S.; Kim, D.; Osuka, A. *Chem.—Eur. J.* **2006**, *12*, 1319.

(14) (a) Cho, S.; Yoon, M.-C.; Kim, C. H.; Aratani, N.; Mori, G.; Joo, T.; Osuka, A.; Kim, D. *J. Phys. Chem. C* **2007**, *111*, 14881. (b) Ahn, T. K.; Kim, K. S.; Kim, D. Y.; Noh, S. B.; Aratani, N.; Ikeda, C.; Osuka, A.; Kim, D. *J. Am. Chem. Soc.* **2006**, *128*, 1700. (c) Cho, H. S.; Song, J. K.; Ha, J.-H.; Cho, S.; Kim, D.; Yoshida, N.; Osuka, A. *J. Phys. Chem. A* **2003**, *107*, 1897.

(15) Osuka, A.; Shimidzu, H. *Angew. Chem., Int. Ed. Engl.* **1997**, *36*, 135.

(16) (a) Hata, H.; Shinokubo, H.; Osuka, A. *J. Am. Chem. Soc.* **2005**, *127*, 8264. (b) Ogawa, T.; Nishimoto, Y.; Yoshida, N.; Ono, N.; Osuka, A. *Angew. Chem., Int. Ed.* **1999**, *38*, 176.

(17) Koide, T.; Kashiwazaki, G.; Suzuki, M.; Furukawa, K.; Yoon, M.-C.; Cho, S.; Kim, D.; Osuka, A. *Angew. Chem., Int. Ed.* **2008**, *47*, 9661.

(18) Yoshida, N.; Ishizuka, T.; Osuka, A.; Jeong, D. H.; Cho, H. S.; Kim, D.; Matsuzaki, Y.; Nogami, A.; Tanaka, K. *Chem.—Eur. J.* **2003**, *9*, 58.

(19) (a) Gouterman, M. *J. Mol. Spectrosc.* **1961**, *6*, 138. (b) Dolphin, D. *The Porphyrins vol.III Physcal Chemistry, Part A*; Academic Press: New York, 1978.

(20) Kasha, M.; Rawls, H. H.; El-Bayoumi, M. A. *Pure Appl. Chem.* **1965**, *11*, 371.

(21) Kim, Y. H.; Jeong, D. H.; Kim, D.; Jeoung, S. C.; Cho, H. S.; Kim, S. K.; Aratani, N.; Osuka, A. *J. Am. Chem. Soc.* **2001**, *123*, 76.

(22) (a) D'Souza, F.; Maligaspe, E.; Karr, P. A.; Schumacher, A. L.; Ojaimi, M. E.; Gros, C. P.; Barbe, J.-M.; Ohkubo, K.; Fukuzumi, S. *Chem.—Eur. J.* **2008**, *14*, 674. (b) Lehtivuori, H.; Lemmetyinen, H.; Tkachenko, N. V. *J. Am. Chem. Soc.* **2006**, *128*, 16036. (c) Li, W.-S.; Kim, K. S.; Jiang, D.-L.; Tanaka, H.; Kawai, T.; Kwon, J. H.; Kim, D.; Aida, T. *J. Am. Chem. Soc.* **2006**, *128*, 10527.

(23) Duvanel, G.; Grilj, J.; Schuwey, A.; Gossauer, A.; Vauthey, E. *Photochem. Photobiol. Sci.* **2007**, *6*, 956.

JP904666S